Supporting Information: Generation of pure OAM beams with a single state of polarization by antenna-decorated microdisk resonators

Kévin G. Cognée,[1,2] Hugo M. Doeleman,[3,1] Philippe Lalanne,[2] and A. Femius Koenderink[1,3]

[1] *Center for Nanophotonics, AMOLF, Science Park 104, 1098 XG Amsterdam, The Netherlands*
[2] *LP2N, Institut d'Optique Graduate School, CNRS, Univ. Bordeaux, 33400 Talence, France*
[3] *Van der Waals-Zeeman Institute, University of Amsterdam, Science Park 904, PO Box 94485, 1090 GL Amsterdam, The Netherlands*

This supplement contains:

- 7 pages, including this cover page
- Figures S1, S2, S3 and S4
- Table S1

CONTENTS

I. MODE STRUCTURE ANALYSIS

Here we discuss the hybridization of N antennas and WGM modes of order m. In particular we demonstrate that accounting for the modal properties of the cavity does not change the rational between the scattered OAM number, the number of antenna N and azimuthal number m. To this end, it is useful to first examine the physics of a ring of radially oriented dipoles concentric with the z-axis of an arbitrary cylindrically symmetric system (be it free space, or a micro disk). For highly symmetric ensembles in plasmonics, group theory has been shown to be a powerful tool for identifying irreducible representations [1, 2]. In a regular ring array of antennas, the analysis is even simpler as the modes complex eigenfrequencies and eigenstates can be obtained analytically [3–5].

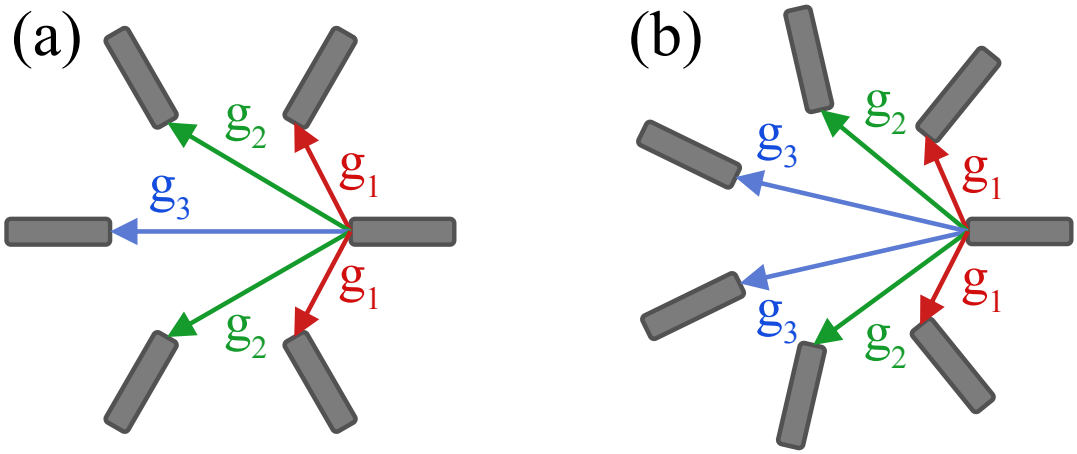

FIG. S1. Sketch of the coupling between regularly spaced antennas arranged on a ring, with an even (a) or odd (b) number of elements.

We consider the geometry of the system described in Figure S1, and assume that dipole i in the chain is solely driven by the interaction with all the other particles in the chain neighbors $p_i = \epsilon_0 \alpha(\omega) \sum_{j\neq i} E_{j\to i}$. Here $\alpha(\omega)$ is the polarizability of the (identical) antennas (normalized by ϵ_0) and the fields $E_{j\to i} = \frac{\omega^2}{c^2} G(\mathbf{r}_j, \mathbf{r}_i, \omega) p_j$ are specified by some Green function. The set of dipole moments is specified by a linear system

$$\mathbf{M}(\omega)\mathbf{p} = \mathbf{0}, \tag{S1}$$

with $\mathbf{p} = [p_1, p_2, \cdots]^T$ and the interaction matrix $\mathbf{M}(\omega)$ of symmetric circulant form generated by the vector $\mathbf{c} = [\alpha^{-1}, g_1, g_2, \cdots, g_2, g_1]$, where we defined $g_n(\omega) = -\frac{\omega^2}{c^2} G(\mathbf{r}_i, \mathbf{r}_{i+n}, \omega)$. The fact that the right hand side of Eq.(S1) is set to zero signifies the fact that we consider the ring in absence of any external driving field. The matrix $\mathbf{M}(\omega)$ being circulant, it can be diagonalized for all (complex) ω

$$\mathbf{M}(\omega)\mathbf{v}_k = \lambda_k(\omega)\mathbf{v}_k, \tag{S2}$$

with k an integer constrained to the interval $k \in [\![-\lfloor \frac{N}{2} \rfloor; \lfloor \frac{N}{2} \rfloor]\!]$. Here we have introduced the eigenvectors:

$$\mathbf{v}_k = \frac{1}{\sqrt{N}} \left[1, e^{i\frac{2\pi}{N}k}, e^{i2\frac{2\pi}{N}k}, \ldots, e^{i(N-1)\frac{2\pi}{N}k}\right]^T,$$

and also the corresponding eigenvalues

$$\lambda_k(\omega) = \alpha^{-1}(\omega) + g_1(\omega)e^{i\frac{2\pi}{N}|k|} + g_2(\omega)e^{i2\frac{2\pi}{N}|k|} + \ldots + g_1(\omega)e^{i(N-1)\frac{2\pi}{N}|k|}. \tag{S3}$$

The eigenvectors are independent of the specific form of the Green function, the diagonalization is valid at any frequency, and thus eigenvectors are not generally to be interpreted as modes (in the sense of quasinormal modes). Note that the eigenvalues are identical (degenerate) for $-k$ and $+k$, and that the eigenvector then correspond to counter-propagating whispering gallery mode. Solving for resonances of the ring Eq.(S1) is equivalent to looking for the frequencies where null eigenvalues occur, which according to Eq (S2), corresponds to

$$\lambda_k(\omega) = 0. \tag{S4}$$

Each value of complex ω respecting this condition is a (complex) resonance frequency with corresponding antenna eigenstate $\mathbf{v}_k$.

Since the eigenvalues $\lambda_k(\omega)$ come in pairs only depending on the absolute value $|k|$, also the resonance frequencies come in pairs, except for the unpaired k-value $k = 0$, and if N is even, $k = \frac{N}{2}$. For even N, we obtain $\frac{N}{2} - 1$ pairs of twice-degenerate modes and two non-degenerate modes. The two non-degenerate modes correspond to the extremal k-values $k = 0$ and $\frac{N}{2}$.

Near a whispering gallery mode resonance of order m, the Green function can be expanded over a set of QNMs [6]. If we consider a single pair of WGMs of azimuthal mode number m, we find that

$$g_n(\omega) \approx \frac{1}{\mu_0 c^2} \frac{\tilde{\omega}_m \tilde{E}_m^2}{\omega - \tilde{\omega}_m} \cos(m\Delta\phi_n), \tag{S5}$$

where $\Delta\phi_n = 2\pi \frac{n}{N}$ represents the angular separation between an antenna and its n^{th} neighbour. Inserting this expression for g_n in Eq.(S3) we obtain for even N,

$$\lambda_k(\omega) = \alpha(\omega)^{-1} + \frac{1}{\mu_0 c^2} \frac{\tilde{\omega}_m \tilde{E}_m^2}{\omega - \tilde{\omega}_m} \left[1 + (-1)^{m+k} + \sum_{n=1}^{\frac{N}{2}-1} \cos\left(2\pi \frac{m+k}{N} n\right) + \cos\left(2\pi \frac{m-k}{N} n\right) \right], \tag{S6}$$

and for odd N,

$$\lambda_k(\omega) = \alpha(\omega)^{-1} + \frac{1}{\mu_0 c^2} \frac{\tilde{\omega}_m \tilde{E}_m^2}{\omega - \tilde{\omega}_m} \left[1 + \sum_{n=1}^{\lfloor \frac{N}{2} \rfloor} \cos\left(2\pi \frac{m+k}{N} n\right) + \cos\left(2\pi \frac{m-k}{N} n\right) \right]. \tag{S7}$$

By analysing these equations, we identify three scenarios:

a). Generically, neither $m + k$ nor $m - k$ are divisible by N, leading to

$$\lambda_k(\omega) = \alpha(\omega)^{-1}.$$

b). $m + k$ and $m - k$ can be simultaneously divisible by N in which case

$$\lambda_k(\omega) = \alpha^{-1}(\omega) + N \frac{1}{\mu_0 c^2} \frac{\tilde{\omega}_m \tilde{E}_m^2}{\omega - \tilde{\omega}_m}.$$

c). When only $m + k$ or $m - k$ is divisible by N, but not both, we have

$$\lambda_k(\omega) = \alpha^{-1}(\omega) + \frac{N}{2} \frac{1}{\mu_0 c^2} \frac{\tilde{\omega}_m \tilde{E}_m^2}{\omega - \tilde{\omega}_m}. \tag{S8}$$

Since k must lie in the irreducible range $[\![-\lfloor \frac{N}{2} \rfloor; \lfloor \frac{N}{2} \rfloor]\!]$, only a single k can respect either b) or c) for a chosen cavity mode number m and a set N. These cases can be understood as follows.

- For the collective antenna modes of case a), the effective polarizability of the antennas is not perturbed at all by the cavity, which implies that these collective antenna modes are decoupled from the cavity. In this work we will only consider scenarios that address the antennas *through* the cavity. Hence, the uncoupled collective antenna modes are irrelevant.

- Case b), occurs particularly when the number of antennas N exactly equals the azimuthal mode order of the cavity modes. In this case the degeneracy of the two cavity modes is lifted in the standing wave basis. The $\cos m\phi$ standing mode is maximally perturbed because all antennas are located at the maximum of the mode profile, and each mode profile maximum has an antenna in it. The dipole moment either points in the same direction as the cavity field (always radial at $k = 0$), or alternates from dipole to dipole for $k = \frac{N}{2}$. The $\sin m\phi$ mode is not perturbed by the antennas, since they are located at the nodes of the mode field.

- In case c), both cavity modes are perturbed by the antennas, but both are shifted in equal amounts so that the degeneracy remains. Assuming (without loss of generality) that $m > 0$ $k > 0$, if $m - k$ is divisible by N, then the cavity mode of mode number m couples to antenna mode k, and conversely cavity mode $-m$ coupled to antenna mode $-k$. This is the basis for literature reports on OAM generation by microring systems. For instance, Cai et al. report in [7] on the simplest case where $m - k = N$, and they show that their devices emit an OAM of $\ell = k$ (± 1 for right/left circular polarization, cf. previous subsection). If instead $m + k$ is divisible by N, the cavity mode m will couple to antenna mode $-k$ (and $-m$ to k).

To conclude this classification, our analysis shows that even though, in principle a ring of N antennas has N eigenmodes, most of these are decoupled from WGM of order m, with the exception of either one or two modes. The scenario for the coupled modes depends on the arithmetic relationship between m and N. The first scenario occurs exactly when N and m are equal or satisfy a commensurate relationship, the antennas lift the WGM mode degeneracy, leaving one unperturbed standing wave mode and one strongly shifted standing wave mode. The induced distribution of dipole moments carries no azimuthal phase gradient. The second experimentally relevant scenario occurs when m and N are not quite equal. Both WGMs are equally shifted and remain degenerate while coupling to eigenmodes with angular momentum $\pm k$ set by the difference between m and N.

II. DESIGN OF EXPERIMENT

In this section we discuss the requirements for actual experimental realizations according to full wave simulations, going beyond the simplifications of our model.

A. Antennas

The predictions discussed in the main paper all consider antennas to be point dipole scatterers that are polarizable along just a single axis. Nanorod antennas will provide an anisotropic polarizability dominantly along their long axis when used at the long-axis resonance frequency, but with a weak residual short axis polarizability. We preferably reach a design for a nanorod antenna where resonances are sufficiently separated such that an appreciable anisotropy between the short and long axis polarizability arises (contrast of order $|\alpha_{long}/\alpha_{short}|^2 > 100$). Furthermore, these objects need to remain small compared to the wavelength of the drive field in the microdisk[8]. This criterion excludes high-index dielectric particles. We therefore turn to metallic antennas, where the surface plasmon confinement allows for small resonant objects, with however the downside of optical absorption. Due to the high plasma frequency of aluminum, aluminium nanorods can be made resonant along their long axis in our laser range for aspect ratio as large as 3-4, as compared to an aspect ratio of just two for gold rods with the same long-axis resonance frequency. Thus, aluminium allows for a 10× higher anisotropy $|\alpha_{long}/\alpha_{short}|^2$ of the polarizability compared to gold antennas. The disadvantages of aluminium are the inter-band absorption at 780 nm, and the grain size of evaporated metal for nanolithographic fabrication, detrimental for the optical quality of our nanostructures.

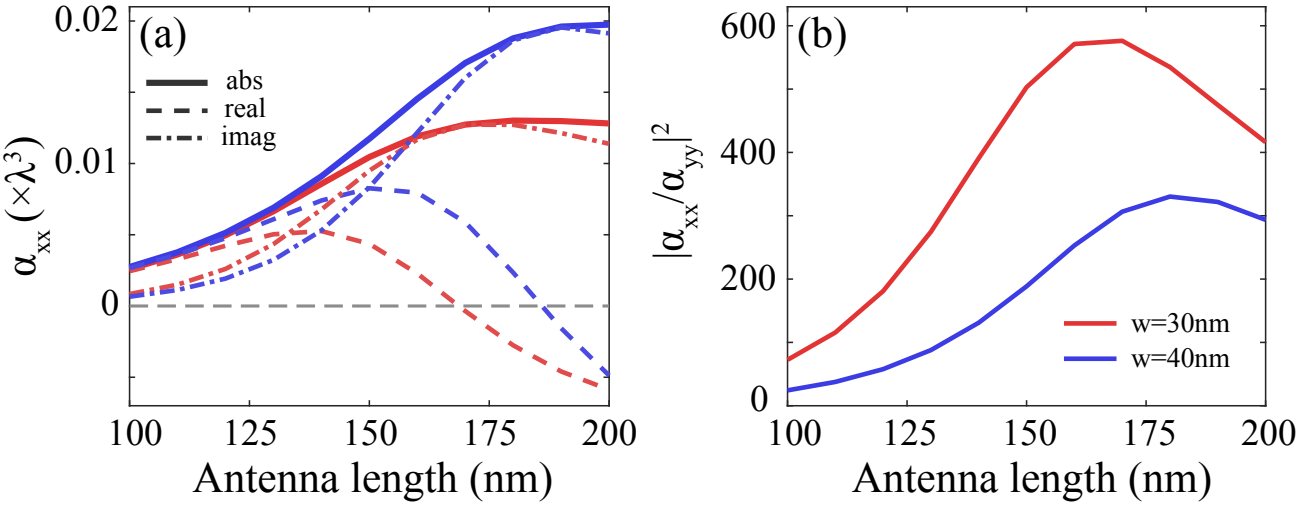

FIG. S2. Polarizability of a 30 nm thick aluminium nanorod antenna on glass at $\lambda = 770$ nm for varied length and width. Red lines are for antenna width of 30 nm, blue are for width of 40 nm (a) Element of diagonal element $\alpha_{x,x}$ along the antenna long axis, solid lines are $|\alpha_{x,x}|$, dashed lines are real($\alpha_{x,x}$) and dash-dotted are imag($\alpha_{x,x}$). (b) Shows the anisotropy between the long and short axis polarizabilities (parallel to the glass plane).

To optimize the shape of our antennas we perform FEM simulations (COMSOL Multiphysics®) of aluminium antennas (tabulated permittivity taken from [9]) placed on an air-glass interface ($n_{glass} = 1.5$). For a fixed thickness of antennas of 30 nm, a width of 30 or 40 nm (to account for fabrication imprecision) and a wavelength of operation of 773 nm, we calculate the polarizability of antennas along their long and short axis (both parallel to the glass interface).

Figure S2 summarizes our simulations. We see in Fig. S2(a) that wider antennas have a stronger polarizability, even though they resonate for longer dimensions (change of sign of real part of α_{xx}). However, Fig. S2(b) suggests that the anisotropy between short and long axis polarizability is most favorable for narrower antennas. To have an appreciable anisotropy (> 100) we need to be close to the resonance of the nanorod. To obtain an anisotropy > 100, with antennas as small as possible, we chose to design our samples with 140 nm long, 30 nm thick and between 30 and 40 nm wide antennas (precise width is difficult to control in fabrication). Such antennas will be somewhat blue-detuned from our cavities operating at $765-781$ nm, which mitigates the broadening of cavity resonances (α_{xx} is mostly real according to Fig. S2(a)).

B. Cavity

The cavities for this study are silicon nitride (Si_3N_4) microdisks. Our fabrication is limited to a fixed 200 nm thickness, given by our wafers (Lionix BV, The Netherlands, 200 nm nitride on oxide, on silicon) and the disks must be wider than 3 µm in diameter to allow for the fabrication of a pillar holding the structure such that the whispering gallery mode decouples from the underlying silicon substrate. In addition to these fabrication constraints, we also add the constraint of our experiment. As explicit in the Bessel function shaped radiation pattern for OAM radiated by rings of dipoles, the beam radiated by a ring of antennas will have an opening angle (maximum of first fringe) which is directly related to the radius of the ring of antennas, and therefore to the radius of the supporting microdisk. This means that the bigger the disk, the narrower the features in the far-field. A 10 µm wide disk would have an opening angle for the first fringe of only 2.6° for OAM of $\ell = \pm 1$, whereas the resolution of our Fourier microscope is only 0.6° per pixel. Therefore we choose to use disks of around 4 µm diameter, which give a fringe diameter of 6.6° for OAM of $\ell = \pm 1$. Such disks would support TE WGM where the fundamental radial mode has an azimuthal mode number in the range of $m = 20-25$. This means that we need almost as many antennas on the disk to create an OAM of $\ell = 0$ to $+3$.

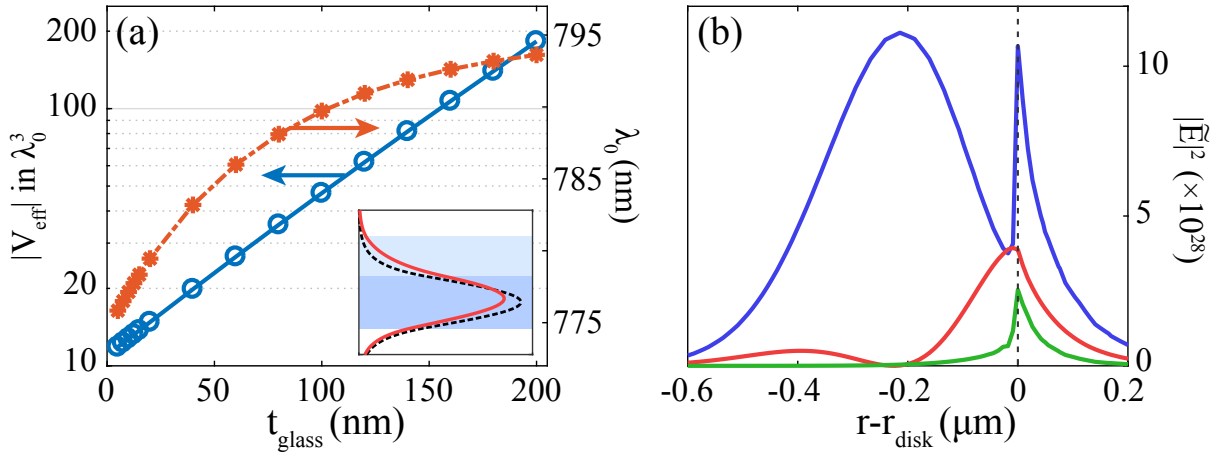

FIG. S3. Mode volume and normalized electric field at the glass-air interface of a microdisk cavity (radius 2 µm, $t_{Si_3N_4} = 200$ nm, mode $m = 22$). (a) Effective mode volume (in unit of wavelength) at the maximum of the field at glass-air interface (solid blue), and resonance wavelength (dashed orange) as a function of top glass layer thickness. The mode volume exponentially increases as we increase the glass layer thickness ($n = 1.5$) as the glass-air interface is moving away from the Si_3N_4 where the field remains confined. The inset shows in dashed black the normalized field intensity of the mode for the symmetric Si_3N_4 cavity ($t_{glass} = 0$) and in red for $t_{glass} = 150$ nm. Since away for the core the mode field is decreasing exponentially, the mode is feeling less and less the perturbation by additional glass thickness and therefore the resonance wavelength converges towards ≈ 795 nm. (b) Normalized intensity of the 3 components of the cavity electric field $m = 22$ at the glass-air interface for $t_{glass} = 150$ nm: blue is $|\tilde{E}_r|^2$, red $|\tilde{E}_{phi}|^2$ and green is $|\tilde{E}_z|^2$. We note that 230 nm from the edge of the disk, the field is maximal on its radial component and minimal on the other two.

C. Antenna-cavity coupling strength

An important design criterion is the linewidth of the cavity resonance once antennas are placed on top on it. We estimate from our perturbation theory from the imaginary part of the polarizability of our antennas (Fig. S2(a)) and

Device type	LHCP:RHCP	OAM peak ratio	nominal OAM versus all other channels
radial	50:50 ± 10	47:53± 3	32+37=69 : 31 ± 6
V-type	85:15 ± 8	95:5 ± 2	62:38 ± 6
Λ-type	33:67 ± 25	19:81 ± 12	53:47 ± 15

TABLE I. Average performance for radial, V-type and Λ type devices, reporting on the LHCP to RHCP polarization ratio, the OAM peak ratio, and the strength of the nominal OAM versus all other channels. For the polarization ratio we consider the sum of all OAM channels in LHCP, and compare to the sum of all OAM channels in RHCP, meaning that 'parasitic' OAM contributions are included. For the OAM peak ratio we list the relative strength of the OAM $m-N-1$ LHCP and $m-N+1$ RHCP peak, i.e., the only two peaks which according to strict selection rules are expected to have amplitude. Balanced amplitude is expected for radial antennas. The V-type antenna shows the best suppression (95:5 ratio on average) of one of the two OAM channels. For the final column, for the radial devices we compare the sum of the OAM $m-N-1$ LHCP and $m-N+1$ RHCP peak to the content of all other channels, while for V- resp. Λ type antenna we compare only the $m-N-1$ resp. $m-N+1$ peak to the sum of all other channels. Averages are over all devices except $m-N=0$, which nominally should not provide OAM. Listed errors are the standard deviation.

an effective mode volume of $V_{\text{eff}} \approx 10\lambda^3$ that 20 antennas placed directly on the disk would broaden the linewidth of the cavity by 4 THz, and therefore limit the quality factor of the system to $Q < 100$. An antenna-dominated low-Q is not a problem *per se* in the sense that for the experiment it is required that the losses of our system are dominated by antenna radiation. However, we do need a clear separation between resonances of different m. This means a linewidth broadened by the antennas to the level that it becomes on the order of the free-spectral range of the cavity is undesirable. Inserting a low refractive index spacer in between the disk and the antennas would allow to raise the antennas out of the mode profile, and thereby provides control over the cavity Q. Compatible with established fabrication is to evaporate a layer of glass ($n_{glass} \approx 1.5$, when $n_{Si_3N_4} \approx 2.0$) on the disks prior to fabricating the antennas. To reach a Q of at least 1000 for the system at hand, we need to increase V_{eff} by a factor of at least ~ 10. Figure S3(a) shows that for the fundamental TE mode for $m = 22$ of disk of 4 µm diameter, 200 nm of Si_3N_4, this is possible for a glass layer thickness of > 120 nm. In this scenario one does need to compensate for a shift in the resonance wavelength of the cavity due to the glass layer (using different disk radius and/or higher mode number m). Finally, one needs to place the antennas in terms of their *radial* position well within the mode profile of the cavity since to benefit optimally from the polarizability anisotropy a purely radial polarization of the mode at the antenna ring must be ensured. In Figure S3(b), for a disk of 4 µm, with 150 nm of glass we see that if we want the cavity field (at the air-glass interface) to be only radial at the position of the antennas, the antennas must be placed 230 nm from the edge of the disk.

III. OAM DECOMPOSITION OF EXPERIMENTAL DATA

Figure S4 presents OAM decomposition histograms for all of the devices underlying Figure 8 in the main manuscript. The histograms report values P_ℓ as function of OAM index ℓ for LHCP and RHC detection (blue resp. red), with the total in each histogram (i.e. blue *plus* red bars, both polarizations) summing to 1. Columns group devices of identical $m-N=-1,0,1,2,3$ (m azimuthal WGM mode quantum number, and N number of antennas), while rows group the radial, V-type and Λ-type devices. We tabulate performance metrics in Table I. These include the polarization contrast LHCP to RHCP summing over all OAM channels, the ratio between the OAM $m-N-1$ LHCP and $m-N+1$ RHCP peak that are the target peaks of the devices according to the selection rule, and the ratio between the 'target' peak and all other OAM channels. This last metric is limited by disorder in the size of our antennas, which causes a speckle pattern, which distributes into parasitic OAM orders. These statistics disregards the $m-N=0$ devices, since those are not expected to generate OAM. Quoted errors are standard deviation to indicate the variability in devices, and not to indicate the uncertainty in the mean.

[1] J. E. Rosenthal and G. M. Murphy, Rev. Mod. Phys. **8**, 317 (1936).
[2] N. A. Mirin, K. Bao, and P. Nordlander, J. Phys. Chem. A **113**, 4028 (2009).
[3] R. M. Kerber, J. M. Fitzgerald, D. E. Reiter, S. S. Oh, and O. Hess, ACS Photonics **4**, 891 (2017).
[4] R. M. Kerber, J. M. Fitzgerald, S. S. Oh, D. E. Reiter, and O. Hess, Commun. Phys. **1**, 87 (2018).
[5] H. H. Jen, M.-S. Chang, and Y.-C. Chen, Sci. Rep. **8**, 9570 (2018).
[6] P. Lalanne, W. Yan, K. Vynck, C. Sauvan, and J.-P. Hugonin, Laser Photonics Rev. **12**, 1700113 (2018).

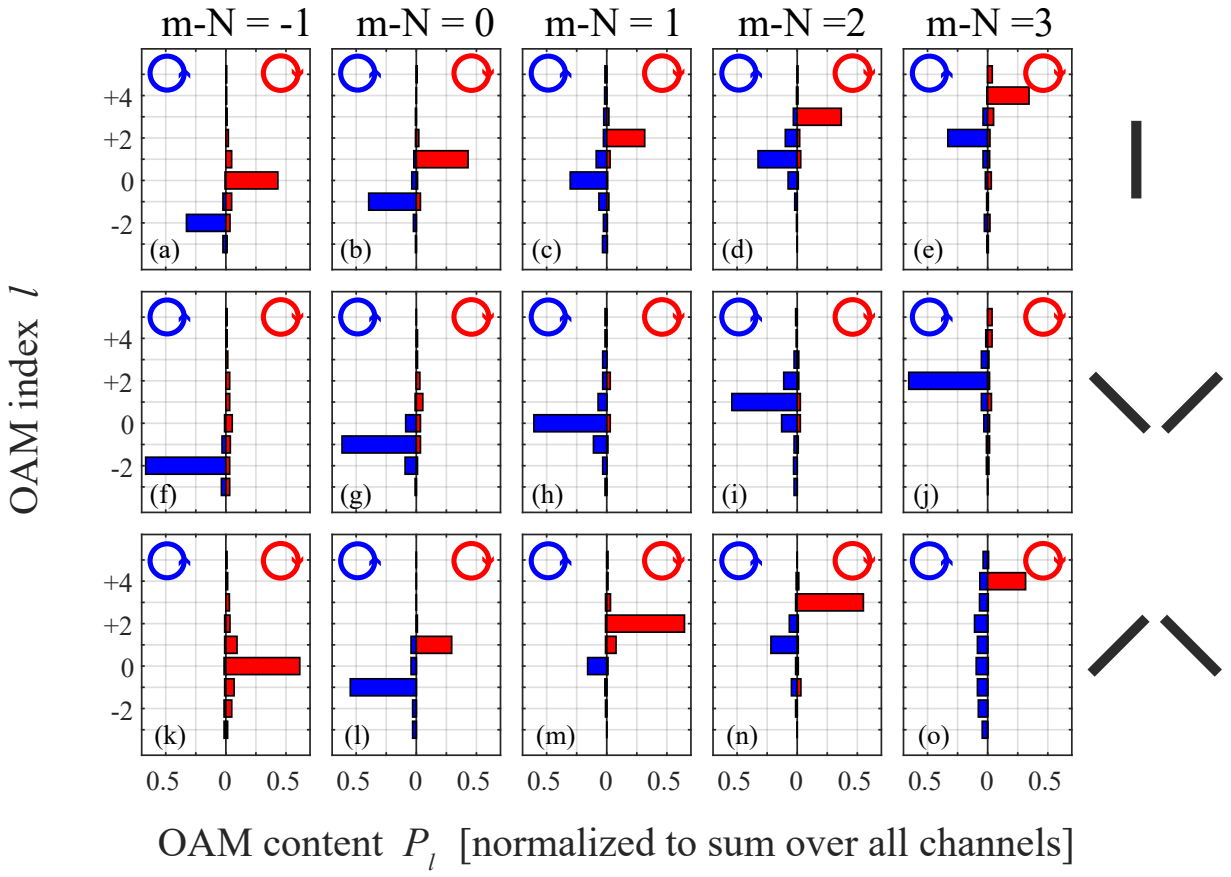

FIG. S4. OAM modal decomposition plotted as individual histograms for all devices underlying Figure 8 in the main manuscript. The top resp. middle and bottom row report on radial (panels a-e), V-type (panels f-j) resp. Λ-type antennas (panels k-o) while columns enumerate $m - N$, i.e., the difference in azimuthal quantum number m of the WGM mode, and N the number of antennas on the device ($m - N = -1$ for panels (a,f,k), $m - N = 0$ for panels (b,g,l), $m - N = 1$ for panels (c,h,m), $m - N = 2$ for panels (d,i,n) and finally $m - N = 2$ for panels (e,j,o). In each diagram LHC reported as blue columns, extending leftwards from the diagram central vertical axis, while RHC is plotted as red columns, extending rightwards. Each histogram is normalized to the sum total of red plus blue columns, meaning that bars represent OAM content relative to the sum total of all channels that compose the beam.

[7] X. X.-L. Cai, J.-W. U. o. B. J. Wang, M. J. Strain, B. Johnson-Morris, J.-B. J. Zhu, M. Sorel, J. L. O'Brien, M. G. Thompson, and S. S.-Y. Yu, Science **338**, 363 (2012).
[8] The effective wavelength inside the cavity is 550 nm, for spectral range of interest set by our laser (765 − 781 nm).
[9] A. D. Rakić, A. B. Djurišić, J. M. Elazar, and M. L. Majewski, Appl. Opt. **37**, 5271 (1998).